Medical Dosimetry 44 (2019) 74–82

Medical Dosimetry

journal homepage: www.meddos.org

Effects of heterogeneities in dose distributions under nonreference conditions: Monte Carlo simulation *vs* dose calculation algorithms

Cristiano Queiroz Melo Reis, PhD[a,*], Patricia Nicolucci, PhD[b], Saulo S. Fortes, MSc[a], Leonardo P. Silva, PhD[a]

[a] *Departamento de Física Médica, Instituto Nacional de Câncer José Alencar Gomes da Silva (INCA), Praça da Cruz Vermelha, Rio de Janeiro, RJ 20230-130, Brazil*
[b] *Departamento de Física, Faculdade de Filosofia Ciências e Letras de Ribeirão Preto, Universidade de São Paulo, Av. Bandeirantes 3900, Ribeirão Preto, SP 14040901, Brazil*

ARTICLE INFO

Article history:
Received 28 November 2017
Revised 7 February 2018
Accepted 15 February 2018

Keywords:
Dose calculation algorithms
Heterogeneity correction
Treatment panning systems
Monte Carlo simulation
Radiotherapy

ABSTRACT

The purpose of this study is to evaluate the performance of dose calculation algorithms used in radiotherapy treatment planning systems (TPSs) in comparison with Monte Carlo (MC) simulations in nonelectronic equilibrium conditions. MC simulations with PENELOPE package were performed for comparison of doses calculated by pencil beam convolution (PBC), analytical anisotropy algorithm (AAA), and Acuros XB TPS algorithms. Relative depth dose curves were calculated in heterogeneous water phantoms with layers of bone (1.8 g/cm^3) and lung (0.3 g/cm^3) equivalent materials for radiation fields between 1×1 cm^2 and 10×10 cm^2. Analysis of relative depth dose curves at the water-bone interface shows that PBC and AAA algorithms present the largest differences to MC calculations ($u_{MC} = 0.5\%$), with maximum differences of up to 4.3% of maximum dose. For the lung-equivalent material and 1×1 cm^2 field, differences can be up to 24.3% for PBC, 11.5% for AAA, and 7.5% for Acuros. Results show that Acurus presents the best agreement with MC simulation data with equivalent accuracy for modeling radiotherapy dose deposition especially in regions where electronic equilibrium does not hold. For typical (nonsmall) fields used in radiotherapy, AAA and PBC can exhibit reasonable agreement with MC results even in regions of heterogeneities.

Introduction

Treatment planning constitutes an important part of the whole radiotherapy treatment process, and assuring that it is performed accurately is one of the most important tasks developed by medical physicists.[1,2] A cumulative accuracy of less than or equal to 5% should be achieved through the chain process, which involves simulation, treatment planning, and dose delivery.[3] Within this process, uncertainties in dose calculations should not be greater than 3% for achieving correlation between the prescribed dose and the treatment outcome.[4] The problem of accurately delivering a prescribed dose to a well-defined target volume is basically dependent on 2 factors: the accuracy with which the radiation beam can be calibrated under well-controlled reference conditions in a uniform water phantom and the capability of calculating and correlating the dose at any point of interest within the patient to the calibrated dose.[5] In this sense, dose calculations performed in the clinical routine by commercial treatment planning systems (TPSs) play a crucial role to guarantee that goal.

In the case of photon radiation fields, many TPSs (such as Eclipse from Varian Medical Systems, Palo Alto, CA) still include a pencil beam convolution (PBC) algorithm, which performs dose calculations in homogeneous water-equivalent materials in reasonable time and with acceptable accuracy.[6,7] In these algorithms, the dose is calculated by convolution of a field intensity fluence with the kernel that describes the dose deposition around the primary photon pencil beam in water. In the presence of inhomogeneities, corrections are applied subsequently so that the radius of the field and depth are scaled according to the density of the media. One example of such correction used in PBC is the equivalent tissue-air ratio.[5] However, those algorithms are known to present serious weaknesses when predicting doses in the presence of heterogeneities. These inaccuracies in dose calculations are mainly because PBC algorithm uses a 1-dimensional density correction and therefore does not accurately model secondary electron transport in heterogeneous media, especially in those regions with lack of charged particle equilibrium (CPE).[8-12] This brings up an

* Reprint requests to Cristiano Queiroz Melo Reis, PhD, Departamento de Física Médica, Instituto Nacional de Câncer José Alencar Gomes da Silva (INCA), Praça da Cruz Vermelha, Rio de Janeiro, RJ 20230-130, Brazil.
E-mail address: fisicomelo@yahoo.com.br (C.Q.M. Reis).

https://doi.org/10.1016/j.meddos.2018.02.009
0958-3947/

important issue when dealing with large-density variations such as in lung cancers and using small ($\leq 3 \times 3\,cm^2$) radiation fields.[13,14]

In regions where CPE does not hold, a better estimation of dose distributions became possible with the introduction of convolution-superposition algorithms, which better account for electron transport. One of these algorithms implemented in the Eclipse TPS is the anisotropic analytical algorithm (AAA)[15,16] released in 2005. Similar to PBC, AAA also considers the dose around pencil beams, but its implementation is quite different. In AAA, the contributions from 3 sources—primary photons and contaminating photons and electrons—are separately modeled and, therefore, each source is associated with a fluence, an energy deposition function, and a scatter kernel. In this way, the kernels that model lateral energy scattering are scaled anisotropically using electron density, whereas the energy deposition density functions are submitted to density scaling in the direction of the pencil beams. The convolution of the contributions from the 3 sources provides the total energy deposited by each pencil beam. The superposition of the contributions from the pencil beams provides the final dose. Several papers published in the literature have reported the improved accuracy achieved with the use of such kind of algorithms.[15,17,18]

More recently, the Varian Medical System has implemented into Eclipse TPS the Acuros XB Advanced Dose Calculation. Acuros makes use of a deterministic grid-based Boltzmann transport equation solver, which in turn explicitly solves the linear Boltzmann transport equation. Different from Monte Carlo (MC) methods that solve the coupled system of linear Boltzmann transport equation stochastically through the transport of photons and electron histories, grid-based Boltzmann transport equation solver methods implement discretization of photon and electron fluences in space, energy, and angle to allow a deterministic solution for the radiation transport within matter. Improvements of the method with particular interest for radiotherapy applications have allowed its use for dose calculations with accuracy similar to those obtained with stochastic MC methods and with significantly less computational effort.[19-21] The importance of more accurate algorithms used in TPSs becomes more evident when dealing with modern radiotherapy techniques, which involves the use of small radiation fields and highly different density regions such as those in lung stereotactic body radiotherapy and stereotactic radiosurgery.[22,23]

Based on this, the purpose of this study is to evaluate the performance of dose calculation algorithms widely used in radiotherapy in regions of heterogeneities in comparison with MC simulation for obtaining accurate values for quantities of interest in dosimetry and radiation physics.[24,25]

Methods and Materials

Monte Carlo modeling of the radiation source

A 6-MV photon beam spectrum published in the literature[26] was used in the input-file *user.in* of PENELOPE package 2008 version[27] to simulate a corresponding clinical beam emitted by a VARIAN Trilogy linear accelerator. Simulations were then accomplished with radiation sources assumed to be point sources emitting the corresponding spectrum. Aiming to validate the 6-MV spectrum, percentage depth dose (%dd) curves were simulated according to the geometrical setup described in TG-51[28] and compared with experimental measurements with a PTW Markus chamber. Absorbed doses to water as a function of depth in a $30 \times 30 \times 30\,cm^3$ water phantom were calculated using scoring voxels of 0.025 cm thickness and 2 cm width. The beam quality index tissue-phantom ratio in water at depths of 20 and 10 g/cm^2 was calculated from the ratio of the percent depth-doses at 20 cm and 10 cm depths, ($PDD_{20,10}$)[29] and compared with measurements.

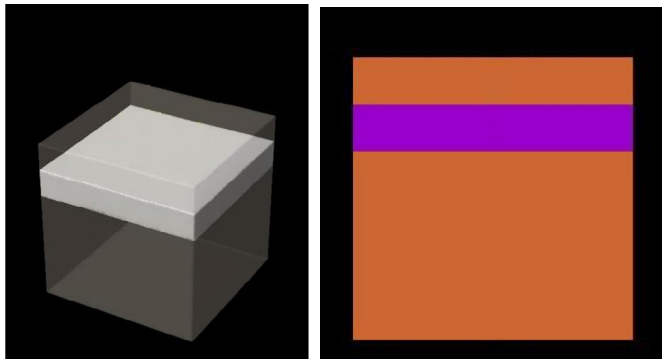

Fig. 1. Virtual heterogeneous water phantom with tissue-equivalent (bone-lung) material interface modeled in the Eclipse treatment planning system (A). In (B) the same setup is modeled with PENELOPE code and visualized using the gview geometry viewer. The tissue-equivalent material slab is 5 cm thick and placed at 5 cm depth in the water phantom. (Color version of figure is available online.)

Dose calculation algorithms in TPS

The algorithms PBC, AAA, and Acuros were first used for calculating adsorbed dose curves relative to the maximum dose in a virtual homogeneous water phantom with $30 \times 30 \times 30\,cm^3$ built in the Eclipse TPS. Absorbed doses to water were calculated for 1 cm × 1 cm, 2 cm × 2 cm, 3 cm × 3 cm, 4 cm × 4 cm, 5 cm × 5 cm, and 10 cm × 10 cm fields at an SSD = 100 cm and using a 0.25 cm grid size. Percentage depth dose curves obtained by the TPS algorithms were then compared with that obtained by MC simulations for the corresponding setup. Virtual heterogeneous water phantoms were also built in Eclipse for investigating the performance of the TPS algorithms in water-lung and water-bone interfaces using computed tomography datasets. In this way, slabs with 5 cm thickness of lung and bone tissue-equivalent materials with densities of 0.3 g/cm^3 (−678 HU) and 1.85 g/cm^3 (1488 HU), respectively, were placed at 5 cm depth within the water phantom as shown in Fig. 1A . The bone density of 1.85 g/cm^3 corresponds to "compact bone" in the International Comission on Radiation Units and Measurements report No. 44.[30] Dose calculations were performed with heterogeneity correction set on and for the same grid size and square fields used with the homogeneous phantom. For the PBC algorithm, calculations were done using the Batho Modified inhomogeneity correction available in Eclipse TPS.

Monte Carlo dose calculations

MC simulations were performed using the PENELOPE package to model the corresponding irradiation geometry used in the Eclipse TPSs. Heterogeneous water phantoms with layers of lung- and bone tissue-equivalent materials were modeled by means of quadric surfaces with the package PENGEOM as shown in Fig. 1B. Cross-section data files for the materials were generated with the corresponding density used in the TPSs. Absorbed doses as a function of depth in the phantoms were calculated using scoring voxels of 0.25 cm thickness and 0.5 cm width and with $N = 1 \times 10^9$ primary histories. Simulation parameters were set to achieve a reasonable compromise between speed and accuracy for all calculations. In this sense, a more detailed simulation was accomplished in the region of interest (dose scoring voxels) defined by a cylinder with 0.3 cm radius (large enough to track electrons in lung material) compared with the simulation for other regions of the phantom. Simulation parameters used to achieve that goal are shown in Table 1.

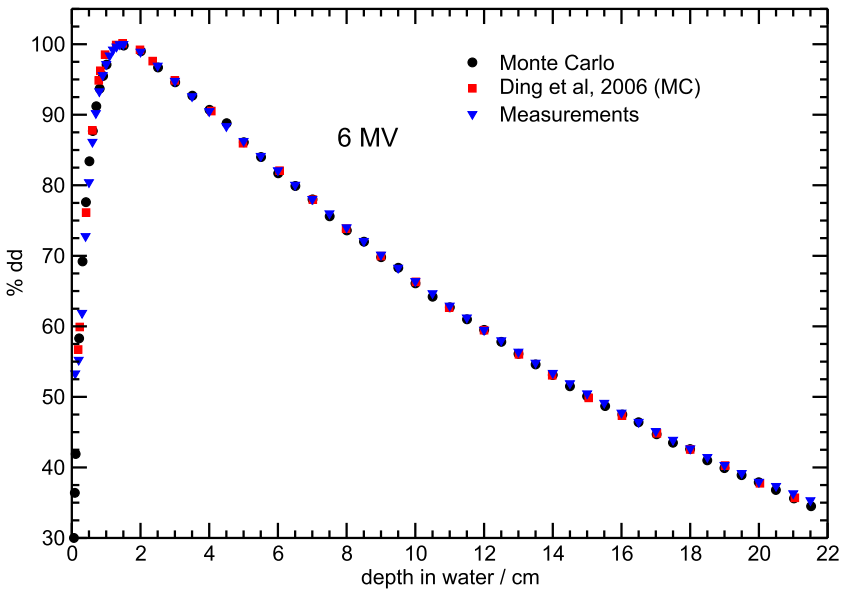

Fig. 2. Percentage depth dose curves in water for a 6 MV photon beam with a $10 \times 10\,cm^2$ field at an SSD = 100 cm. Monte Carlo simulated depth dose calculations are compared with data also obtained by simulation by Ding *et al.*[26] and to experimental measurements with a Markus chamber. (Color version of figure is available online.)

Table 1
Simulation parameters used in this study with PENELOPE code for tracking particles in a heterogeneous water phantom.

Parameters	Water or bone		Lung	
	Central axis	Other regions	Central axis	Other regions
$E_{abs}(e^-, e^+)$	10 keV	100 keV	5 keV	50 keV
$E_{abs}(\gamma)$	5 keV	10 keV	1 keV	5 keV
C_1, C_2	0.02	0.1	0.02	0.1
W_{CC}	10 keV	100 keV	5 keV	50 keV
W_{CR}	5 keV	10 keV	1 keV	5 keV

Parameters C_1 and C_2 account for the average angular deflection and maximum average fractional energy loss between 2 consecutive hard elastic events, respectively. Values of threshold energies for hard inelastic interactions, W_{CC}, hard bremsstrahlung emission, W_{CR}, and absorption energies for electrons, $E_{abs}(e^-)$, positrons, $E_{abs}(e^+)$, and photons, $E_{abs}(\gamma)$, are also shown.

Results and Discussion

Validation of the photon spectrum

Experimental data of the percentage depth dose curve for the 6-MV beam were compared with those calculated by MC and are presented in Fig. 2 for a $10 \times 10\,cm^2$ field. The plots show that our MC results agree with measurements with maximum difference of 0.7% relative to maximum dose after the buildup region. Statistical uncertainties on MC calculations are of 0.5% on average. The calculated value of the beam quality index, $TPR_{20,10}$, of 0.6673 was also found to agree with the value obtained from the $PDD_{20,10}$ measured in the clinical beam with a relative percentage difference of 0.5%. Fig. 2 also shows that our results are in fair agreement with MC data obtained by Ding *et al.*,[26] with maximum difference of 0.4% relative to maximum dose for depths beyond D_{max} .

Depth dose calculations in homogeneous phantom

Fig. 3 shows comparisons of depth dose curves relative to D_{max} calculated with PENELOPE and with the TPS algorithms investigated for 6 square field sizes between $1 \times 1\,cm^2$ and $10 \times 10\,cm^2$. Fig. 3A compares our simulated %dd curve to those obtained by the TPS dose calculation algorithms for a $10 \times 10\,cm^2$ field. The graphs show that for this reference field size, depth doses calculated by the 3 algorithms are in fair agreement with results obtained by MC simulations. Comparisons with MC data provided maximum differences of 1.6%, 1.2%, and 1.1% relative to maximum dose after the buildup region for PBC, AAA, and Acuros, respectively.

Fig. 3F shows the results for the $1 \times 1\,cm^2$ field, which represents the worst scenario for the absence of CPE in the homogeneous water phantom. Comparison of PBC and PENELOPE calculations for depths after the buildup region shows a maximum difference of 2.7% relative to maximum dose. For AAA and Acuros, maximum differences from MC results were 0.8% and 1.3%, respectively. For all the other field sizes shown in Fig. 3, doses calculated by the 3 TPS algorithms were found to agree with MC calculations within 0.9% of the maximum dose on average. Fig. 3 also shows that the largest difference between Acuros and MC simulations is observed for deeper regions in the phantom and for small ($\leq 3 \times 3\,cm^2$) field sizes. That behavior is probably related to the fact that those algorithms have lower accuracy beyond the region of interest for clinical purposes.

Depth dose curves in heterogeneous media

Water-bone interface

Fig. 4 shows %dd curves for the heterogeneous water phantom with compact bone calculated by MC simulations with PENELOPE code in comparison with those obtained with TPS algorithms. We can see from the plots that the algorithms have slightly different behaviors in the 3 different parts of the phantom (in the water before the bone layer was reached, inside the bone, and in the water after the heterogeneity). Average statistical uncertainties on MC data are between 0.1% and 0.9% for the $1 \times 1\,cm^2$ and the $10 \times 10\,cm^2$ fields, respectively. Table 2 shows PDD values for depths within the water-bone interface for the fields investigated in this study.

For depths beyond D_{max} and in the first layer of water before the bone-equivalent medium, all the algorithms were found to agree with MC simulations for all field sizes investigated. The algorithm Acuros, which presented in general the best agreement with MC results, has shown an overprediction of dose in the vicinities of the interface, which causes this algorithm to present the largest difference compared with PENELOPE data in this part of

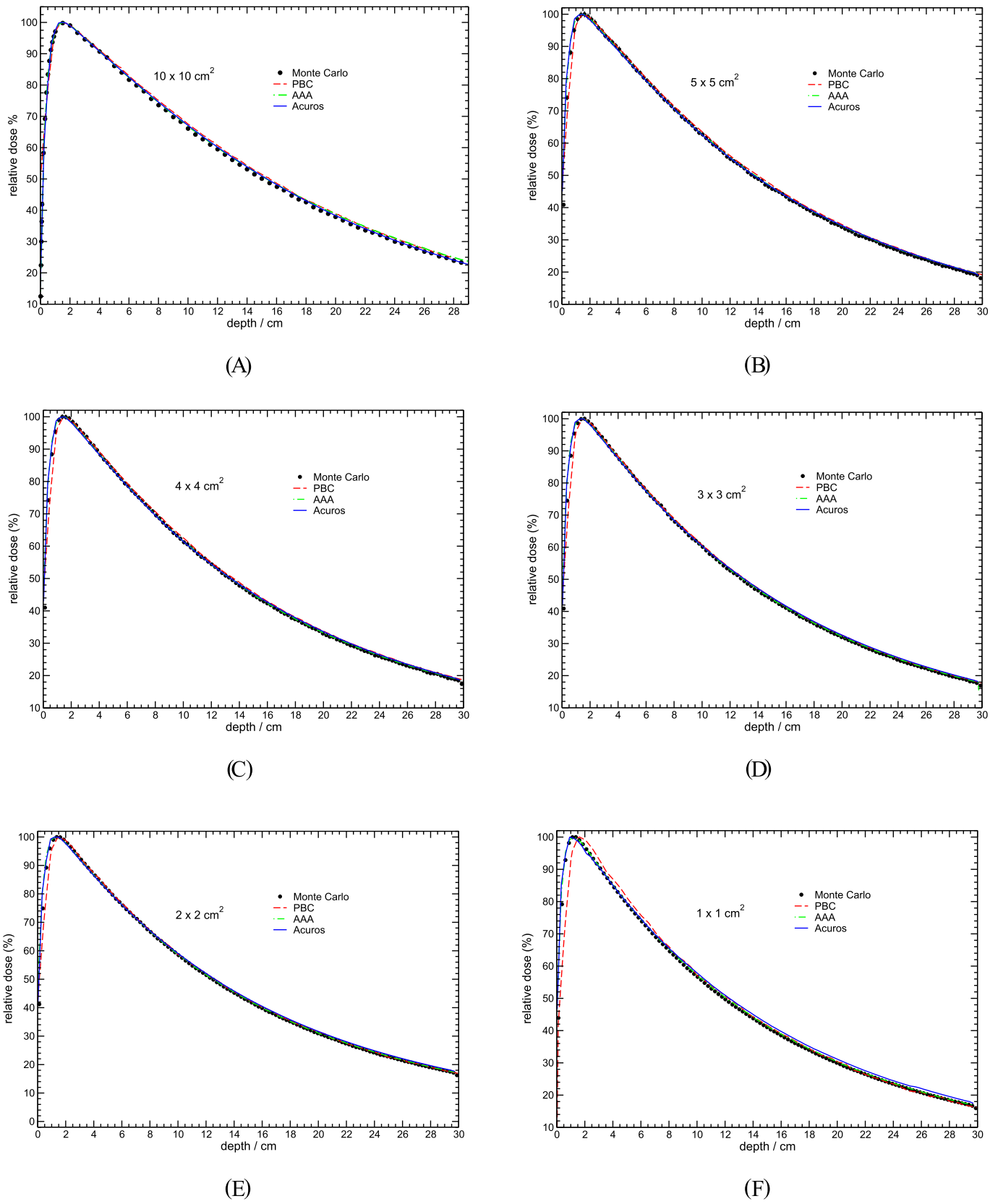

Fig. 3. Percentage depth dose curves in a $30 \times 30 \times 30\,cm^3$ homogeneous water phantom for 6 square field sizes with SSD = 100 cm in 6-MV photon beams. Doses obtained by MC simulation with PENELOPE code are compared with those obtained by the TPS algorithms PBC, AAA, and Acuros. (Color version of figure is available online.)

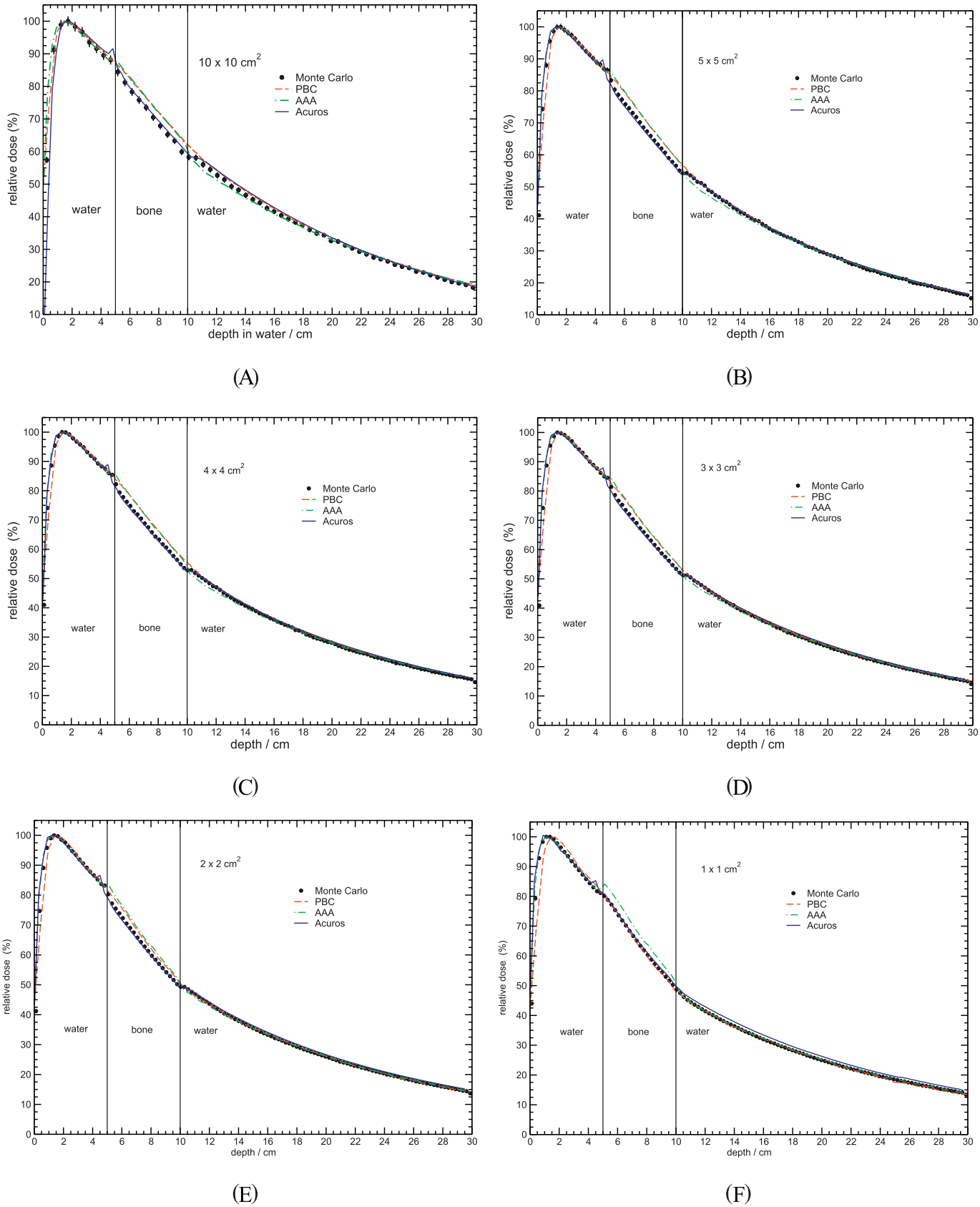

Fig. 4. Six MV %dd curves for the water-bone interface calculated by Monte Carlo simulation with PENELOPE code and with algorithms PBC, AAA, and Acuros. Calculations are for 6 square fields including a $10 \times 10\,cm^2$ reference size and small ($\leq 5 \times 5\,cm^2$) fields. (Color version of figure is available online.)

Table 2
Percentage depth dose values within the water-bone interface calculated by PBC, AAA, and Acuros algorithms in comparison with MC simulations.

Depth (cm)	1×1 cm^2				2×2 cm^2				3×3 cm^2			
	PBC	AAA	Acuros	MC	PBC	AAA	Acuros	MC	PBC	AAA	Acuros	MC
3	92	91	91	90.3 (2)	93	92	92	91.9 (4)	94	93	93	93.1 (6)
4	86	85	86	84.4 (2)	87	87	87	86.6 (4)	88	88	88	87.7 (5)
5	81	84	81	80.1 (2)	82	83	79	80.3 (3)	83	84	80	81.4 (5)
6	74	78	74	73.6 (2)	76	77	72	72.3 (3)	77	78	73	73.5 (4)
7	67	71	68	66.7 (1)	69	70	66	65.8 (3)	71	71	67	67.3 (4)
8	60	64	61	60.3 (1)	62	63	60	59.7 (3)	64	65	61	61.6 (4)
9	54	58	56	54.5 (1)	56	57	54	54.2 (2)	58	59	56	56.2 (4)
10	48	51	50	48.7 (1)	50	51	49	49.3 (2)	53	52	51	51.2 (4)
11	44	44	46	44.4 (1)	46	46	47	46.8 (2)	49	47	49	48.7 (4)
12	41	42	43	41.4 (1)	43	43	44	43.6 (2)	45	44	46	45.3 (3)
Depth (cm)	4×4 cm^2				5×5 cm^2				10×10 cm^2			
	PBC	AAA	Acuros	MC	PBC	AAA	Acuros	MC	PBC	AAA	Acuros	MC
3	94	94	93	93.2 (7)	94	94	94	93.7 (9)	95	95	96	94 (2)
4	89	88	89	88.3 (7)	90	89	89	88.9 (9)	91	90	92	90 (1)
5	84	85	82	82.2 (6)	85	86	82	83.3 (8)	87	88	88	84 (1)
6	79	79	74	74.8 (6)	80	80	75	75.8 (7)	82	83	80	78 (1)
7	72	72	68	68.8 (6)	74	74	70	70.2 (7)	77	77	74	74 (1)
8	66	66	63	63.3 (5)	68	68	64	64.5 (7)	72	72	69	68 (1)
9	61	60	58	57.7 (5)	62	62	59	59.0 (6)	67	67	64	63 (1)
10	55	54	52	52.8 (5)	57	55	54	54.3 (6)	62	61	60	58 (1)
11	51	48	51	50.2 (5)	52	50	52	51.6 (6)	58	56	57	56 (1)
12	47	45	47	47.0 (5)	48	47	49	48.4 (6)	54	51	54	53 (1)

Data for depths inside the bone layer are highlighted in gray. Statistical uncertainties on the final digit for MC calculations are shown in parentheses beside each value.

the phantom. Although that can be related to the backscatter effect of high-Z materials, which has already been well described in the literature,[31,32] our MC calculations show that the effect is not that big for this particular bone-equivalent material in 6-MV photon beams. Maximum difference in this region was of 2.9% (4.8 cm depth) for the algorithm Acuros with a 5×5 cm^2 field.

Analysis of the data inside the bone-equivalent material shows that the algorithm AAA overpredicted the dose for all field sizes used in this study. This can be understood, taking into account that convolution-superposition algorithms such as AAA work better for materials that have atomic numbers close to water (such as lung).[11] This is due to the fact that the initial dose kernels obtained from measurements in water are rescaled based on the physical properties of the medium where the energy is absorbed. In this sense, for mediums with high atomic number, such as bone, the electrons released will be scattered at wider angles due to its higher angular scattering power and therefore the shape of the rescaled kernel as well as the rescalation will not be correct. Similar to what was observed for the AAA, the PBC algorithm also overpredicted the dose inside the bone for all field sizes except for 1×1 cm^2 (Fig. 4F). A possible explanation for that can be the lack of lateral electronic equilibrium for such small field. Considering that 6 MeV electrons have on average a continuous slowing-down approximation range in bone of approximately 2 cm, even the secondary electrons generated in the beam axis have a non-negligible probability of depositing their energy beyond the borders of the field and are not replaced by electrons generated elsewhere within it. This effect seems to be more important for PBC than the overprediction observed for the other field sizes. Doses calculated inside the bone with Acuros presented the best agreement with MC calculations. Maximum difference in this part of the phantom was of 4.3% (at 6 cm depth) for AAA in a 1×1 cm^2 field.

For depths after the interface, all algorithms were found to agree in general with MC simulations. For depths in the vicinity of the bone-water interface, only the Acuros was able to correctly reproduce together with PENELOPE the rebuildup effect caused by differences between the electrons being generated in the bone and those being generated in the water close to the interface. In this part of the phantom, there is a decrease of the number of electrons originated in the bone simultaneously with an increasing of those originated in water. Since electrons generated in bone have wider angle scattering, these 2 effects are not mutually compensating and that difference will cause a buildup of dose. However, we can see from our MC calculations shown in Fig. 4F that this effect is not appreciable for the 1×1 cm^2 field size. Similar to what was observed for the %dd curves calculated in the homogeneous water phantom, the largest differences between doses calculated by Acuros and MC simulations were observed for small fields at deeper regions of the phantom. For the region immediately below the interface, a maximum difference of 3.5% was observed between PBC and MC data for a 10×10 cm^2 field.

Water-lung interface

Fig. 5 shows MC and TPS's calculated %dd curves for the heterogeneous water phantom with a 5 cm thickness slab of lung-equivalent material at 5 cm depth for 6 different square fields in a 6-MV photon beam. Similar to what was observed for the water-bone interface the algorithms presented different behaviors in the 3 different regions of the phantom. Average statistical uncertainties on MC calculations vary from 0.1% to 1.0% for the 1×1 cm^2 and 10×10 cm^2 fields, respectively.

For the region of the phantom before the water-lung interface, Fig. 5 shows that the 4 TPS algorithms agree pretty well with MC calculations for the 6 square fields investigated. Maximum difference observed for this region of the phantom was of 3.1% (at 4.8 cm depth) for Acuros with a 2×2 cm^2 field.

The highest differences between MC and TPS's algorithm calculations were found to be in the lung-equivalent part of the

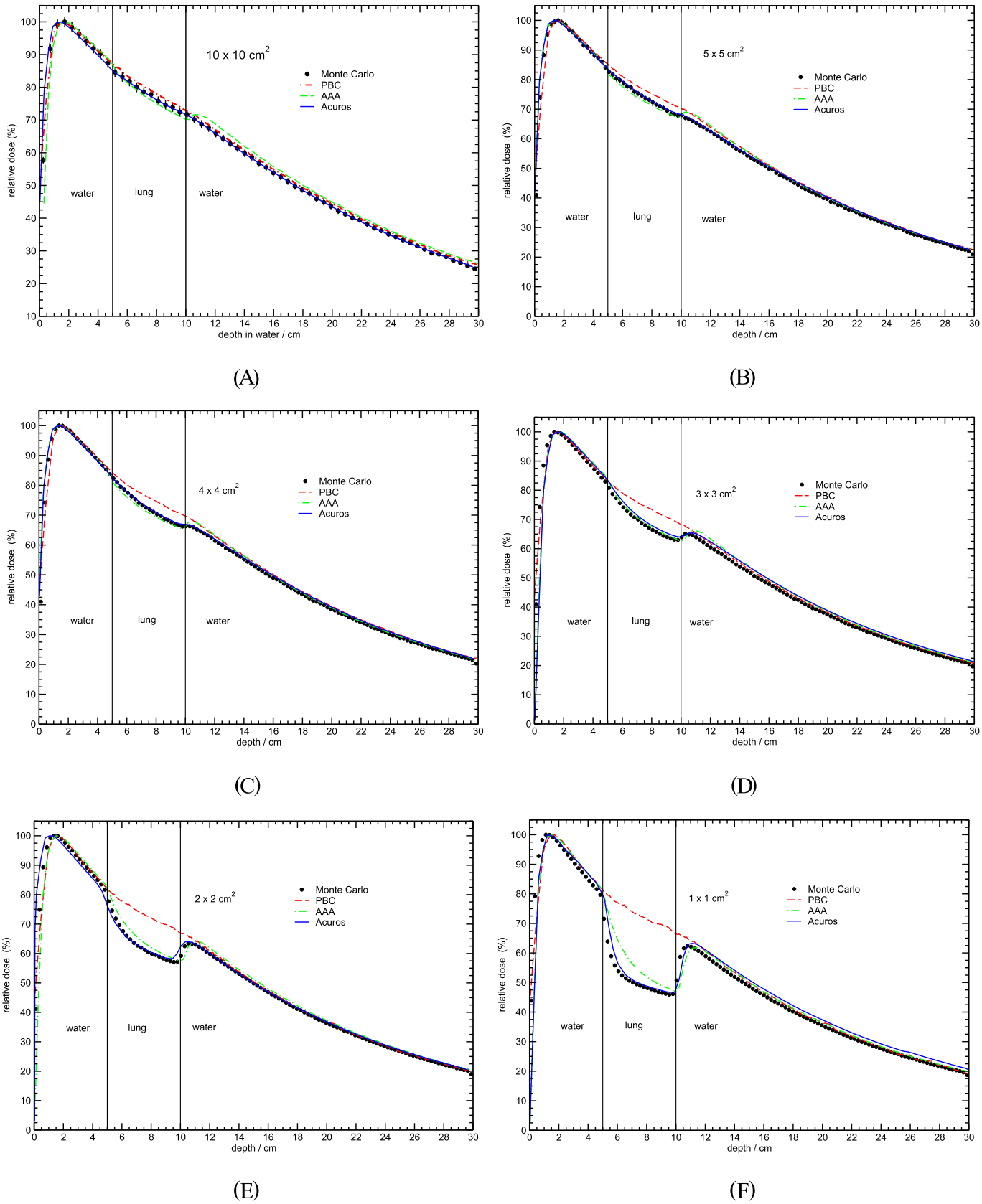

Fig. 5. Comparison of 6 MV relative dose curves in the heterogeneous water phantom with a water-lung interface for a reference $10 \times 10\,cm^2$ field and for fields $\leq 5 \times 5^2$. Graphs show curves calculated with PENELOPE code and TPS algorithms. (Color version of figure is available online.)

Table 3
Percentage depth dose values within the water-lung interface calculated by PBC, AAA, and Acuros algorithms in comparison with MC simulations.

Depth (cm)	1×1 cm^2				2×2 cm^2				3×3 cm^2			
	PBC	AAA	Acuros	MC	PBC	AAA	Acuros	MC	PBC	AAA	Acuros	MC
3	93	93	92	90.2 (2)	93	94	92	92.0 (4)	94	95	94	92.7 (6)
4	87	87	87	84.4 (2)	87	88	86	86.4 (4)	88	90	89	87.2 (5)
5	81	80	79	71.6 (2)	82	82	76	77.7 (4)	83	83	83	80.8 (6)
6	77	64	57	53.8 (1)	78	72	67	67.6 (3)	79	75	76	74.1 (5)
7	74	56	51	50.0 (1)	75	66	63	62.7 (3)	76	71	71	70.0 (5)
8	72	52	49	48.1 (1)	72	62	60	59.8 (3)	73	68	68	66.4 (5)
9	70	49	47	46.5 (1)	70	59	58	57.7 (3)	71	65	65	64.0 (5)
10	66	47	48	50.7 (1)	67	58	62	59.2 (3)	68	63	64	63.9 (5)
11	64	61	63	62.1 (1)	65	64	63	63.0 (3)	66	66	65	63.9 (4)
12	61	60	61	58.9 (1)	61	62	60	59.8 (3)	62	63	62	60.4 (4)
Depth (cm)	4×4 cm^2				5×5 cm^2				10×10 cm^2			
	PBC	AAA	Acuros	MC	PBC	AAA	Acuros	MC	PBC	AAA	Acuros	MC
3	94	94	93	93.1 (7)	94	94	94	93.3 (9)	95	96	94	92 (2)
4	89	88	88	88.1 (7)	90	89	89	88.2 (9)	91	92	90	90 (1)
5	85	81	83	82.3 (7)	85	82	83	82.6 (9)	87	87	85	85 (2)
6	80	76	78	77.5 (7)	81	78	79	78.8 (9)	84	82	82	82 (2)
7	77	72	74	73.3 (7)	78	74	76	75.3 (9)	81	78	79	79 (1)
8	75	69	71	70.3 (7)	75	71	73	72.3 (8)	78	75	76	76 (1)
9	72	67	68	67.6 (7)	73	69	70	69.5 (8)	76	72	74	74 (1)
10	70	66	67	66.3 (6)	70	68	68	68.0 (8)	73	70	72	72 (1)
11	67	67	65	64.6 (6)	67	68	66	65.3 (7)	70	71	69	69 (1)
12	63	63	62	61.4 (6)	64	64	63	62.4 (7)	67	69	66	66 (1)

Data for depths inside the lung layer are highlighted in gray. Statistical uncertainties on the final digit for MC calculations are shown in parentheses beside each value.

phantom as shown in Fig. 5 and Table 3. For fields greater than or equal to 4×4 cm^2 (Fig. 5A–C) where lateral electronic equilibrium is guaranteed, discrepancies can be understood, taking into account that the decrease in the interaction cross section is greater than the increase in transmission within the lung material. This explains the dose overestimation by classical TPS algorithms such as PBC, which do not model the decrease of the interaction coefficient and only account for the increased transmission of radiation in low-density materials. Fig. 5D–F shows that differences become much bigger when dealing with small ($\leq 3 \times 3$ cm^2) fields and when using PBC and AAA for calculating depth doses. That poor agreement with MC calculations is mainly because of the lateral electronic equilibrium loss, which is not appropriately accounted for in none of those 2 algorithms. This effect becomes worse in low-density materials such as lung because of the wider range of Compton electrons producing a characteristic drop in the depth dose curve. For PBC, differences can reach 21.9% on average with a maximum of 24.3% (at 6.6 cm depth) when using a 1×1 cm^2 field. At the same conditions, AAA presented an average deviation of 5.8% and maximum of approximately 11.5% ($z = 5.6$ cm). The best agreement with MC results in the lung part of the phantom was obtained with Acuros for all field sizes used in this study. For a 1×1 cm^2 field, average percentage difference is around 1.9%. A maximum deviation of 7.5% is also observed very close to the the water-lung interface.

For depths in water beyond the lung-water interface, the poorest agreement to MC calculations was obtained for the PBC algorithm for the 1×1 cm^2 field, with maximum percentage difference of 15.6% relative to maximum dose. Acuros presented a maximum deviation of 5.7% for the 1×1 cm^2 field in the same region because of the rebuildup effects immediately after the interface. All the other algorithms were found to agree with MC data in this part of the phantom for all field sizes.

Conclusions

Percentage depth dose curves in homogeneous and heterogeneous water phantom have been calculated for reference and non-electronic equilibrium conditions using TPS algorithms and MC simulations. Results have shown that PBC can get comparable results with more sophisticated algorithms such as AAA and Acuros in homogeneous water phantom or even with bone-equivalent materials within it. However, PBC can drastically overestimate doses in lung-equivalent regions and when using small ($\leq 3 \times 3$ cm^2) fields. The algorithm AAA was found to agree pretty well with MC calculations inside lung for fields greater than 2×2 cm^2, but can overestimate depth doses by up to 11.5% of maximum doses when using fields smaller than that. The algorithm Acuros presented the best agreement with data obtained by MC when calculating absorbed doses in lung and using small radiation fields. Since algorithms totally based in MC methods are still unfeasible in clinical environment, Acuros is found to be the best choice when dealing with treatment techniques in radiotherapy that make use of similar conditions investigated in this study.

Acknowledgment

This work was supported by a scholarship from the Brazilian Ministry of Health—MS held by C.Q.M. Reis.

References

1. Fraass, B.; Doppke, K.; Hunt, M.; *et al.* American Association of Physicists in Medicine Radiation Therapy Committee Task Group 53: Quality assurance for clinical radiotherapy treatment planning. *Med. Phys* **25**:1773–829; 1998.
2. ICRU Report 83: Prescribing, recording, and reporting photon-beam intensity modulated radiation therapy (IMRT). *J ICRU* **10**:1–106; 2010.
3. ICRU. *Prescribing, Recording and Reporting Photon Beam Therapy (Supplement to ICRU Report 50)* ICRU Report 62; ICRU, Washington, DC; 1999.

4. Brahme, A.; Chavaudra, J.; Landberg, T.; *et al.* Accuracy requirements and quality assurance of external beam therapy with photons and electrons. *Acta Oncol. (Madr)*(suppl. 1):1–76; 1988.
5. Papanikolaou, N.; Battista, J.J.; Boyer, A.L.; *et al. Tissue inhomogeneity corrections for megavoltage photon beams* AAPM Report 85; Medical Physics Pub for AAPM, New York; 2004.
6. Ahnesjö, A.; Saxner, M.; Trepp, A. A pencil beam model for photon dose calculation. *Med. Phys* **19**:263–73; 1992.
7. Ali, I.; Ahmad, S. Quantitative assessment of the accuracy of dose calculation using pencil beam and Monte Carlo algorithms and requirements for clinical quality assurance. *Med. Dosim* **38**(3):255–61; 2013.
8. Boyer, A.L.; Mok, E.C. Calculation of photon dose distributions in an inho-mogeneous medium using convolutions. *Med. Phys* **13**:503–9; 1986.
9. Knoos, T.; Ahnesjo, A.; Nilsson, P.; *et al.* Limitations of a pencil beam approach to photon dose calculations in lung tissue. *Phys. Med. Biol* **40**:1411–20; 1995.
10. Carrasco, P.; Jornet, N.; Duch, M.A.; *et al.* Comparison of dose calculation algorithms in phantoms with lung equivalent heterogeneities under conditions of lateral electronic disequilibrium. *Med. Phys* **31**:2899–991; 2004.
11. Carrasco, P.; Jornet, N.; Duch, M.A.; *et al.* Comparison of dose calculation algorithms in slab phantoms with cortical bone equivalent heterogeneities. *Med. Phys* **34**(8):3323–33; 2007. http://dx.doi.org/10.1118/1.2750972.
12. Papanikolaou, N.; Stathakis, S. Dose-calculation algorithms in the context of inhomogeneity corrections for high energy photon beams. *Med. Phys* **36**(10):4765–75; 2009. http://dx.doi.org/10.1118/1.3213523.
13. Jones, A.O.; Das, I.J. Comparison of inhomogeneity correction algorithms in small photon fields. *Med. Phys* **32**(3):766–76; 2005. http://dx.doi.org/10.1118/1.1861154.
14. Aarup, L.A.; Nahum, A.L.; Zacharatou, C.; *et al.* The effect of different lung densities on the accuracy of various radiotherapy dose calculation methods: Implications for tumour coverage. *Radiother. Oncol* **91**:405–14; 2009.
15. Ulmer, W.; Pyyry, J; Kaissl, W. A 3D photon superposition/convolution algorithm and its foundation on results of Monte Carlo calculations. *Phys. Med. Biol* **50**:1767–90; 2005.
16. Bragg, C.M.; Wingate, K.; Conway, J. Clinical implications of the anisotropic analytical algorithm for IMRT treatment planning and verification. *Radiother Oncol* **86**(2):276–84; 2008.
17. Bragg, C.M.; Conway, J. Dosimetric verification of the anisotropic analytical algorithm for radiotherapy treatment planning. *Radiother Oncol* **81**(3):315–23; 2006. http://dx.doi.org/10.1016/j.radonc.2006.10.020 <GotoISI>://WOS:000243210700015.
18. Fogliata, A.; Vanetti, E.; Albers, D.; *et al.* On the dosimetric behaviour of photon dose calculation algorithms in the presence of simple geometric heterogeneities: comparison with Monte Carlo calculations. *Phys. Med. Biol* **52**(5):1363–85; 2007. http://dx.doi.org/10.1088/0031-9155/52/5/011 <GotoISI>://WOS:000244714200011.
19. Vassiliev, O.N.; Wareing, T.A.; McGhee, J.; *et al.* Validation of a new grid-based Boltzmann equation solver for dose calculation in radiotherapy with photon beams. *Phys. Med. Biol* **55**:581–98; 2010. http://stacks.iop.org/0031-9155/55/581.
20. Bush, K.; Gagne, I.M.; Zavgorodni, S.; *et al.* Dosimetric validation of Acuros XB with Monte Carlo methods for photon dose calculations. *Med. Phys* **38**:2208–21; 2011. http://link.aip.org/link/?MPH/38/2208/1.
21. Fogliata, A.; Nicolini, G.; Clivio, A.; *et al.* Dosimetric evaluation of Acuros XB Advanced Dose Calculation algorithm in heterogeneous media. *Radiat Oncol* **6**; 2011. http://dx.doi.org/10.1186/1748-717x-6-82 <GotoISI>://WOS:000294607100001.
22. Huang, B.; Wu, L.; Lin, P.; *et al.* Dose calculation of Acuros XB and Anisotropic Analytical Algorithm in lung stereotactic body radiotherapy treatment with flattening filter free beams and the potential role of calculation grid size. *Radiat Oncol* **10**; 2015. http://dx.doi.org/10.1186/s13014-015-0357-0 <GotoISI>://WOS:000350728500001.
23. Liang, X.; Penagaricano, J.; Zheng, D.; *et al.* Radiobiological impact of dose calculation algorithms on biologically optimized IMRT lung stereotactic body radiation therapy plans. *Radiat Oncol* **11**; 2016. http://dx.doi.org/10.1186/s13014-015-0578-2 <GotoISI>://WOS:000368484900002.
24. Rogers, D.W.O. Fifty years of Monte Carlo simulations for medical physics. *Phys. Med. Biol* **51**:R287–301; 2006.
25. Chetty, I.J.; *et al.* Report of the AAPM Task Group No. 105: Issues associated with clinical implementation of Monte Carlo-based photon and electron external beam treatment planning. *Med. Phys* **34**:4818–53; 2007.
26. Ding, G.X.; Duggan, D.M.; Coffey, C.W. Commissioning stereotactic radiosurgery beams using both experimental and theoretical methods. *Phys. Med. Biol* **51**:2549–66; 2006.
27. Salvat, F.; Fernández-Varea, J.M.; Sempau, J.. *PENELOPE-2008: A Code System for Monte Carlo Simulation of Electron and Photon Transport. Tech. Rep* OECD Nuclear Energy Agency; Issy-les-Moulineaux, France; 2008.
28. Almond, P.R.; Biggs, P.J.; Coursey, B.M.; *et al.* AAPM's TG–51 protocol for clinical reference dosimetry of high-energy photon and electron beams. *Med. Phys* **26**:1847–70; 1999.
29. IAEA. Absorbed Dose Determination in External Beam Radiotherapy: An International Code of Practice for Dosimetry Based on Standards of Absorbed Dose to Water. *of Technical Report Series*, Vol. 398. Vienna: IAEA; 2001.
30. ICRU. *Tissue Substitutes in Radiation Dosimetry and Measurements* ICRU Report 44; ICRU, Washington, DC; 1989.
31. Das, I.J.; Kahn, F.M. Backscatter dose perturbation at high atomic-number interfaces in megavoltage photon beams. *Med. Phys* **16**(3):367–75; 1989.
32. Sauer, O.A. Calculation of dose distributions in the vicinity of high-Z inter-faces for photon beams. *Med. Phys* **22**(10):1685–90; 1995.